AIAA JOURNAL
Vol. 34, No. 7, July 1996

Constrained Layer Damping of Tubular Truss Members

Hamid R. Adib-Jahromi,* Ramesh B. Malla,† and Michael L. Accorsi‡
University of Connecticut, Storrs, Connecticut 06269-2037

An efficient technique is developed to model tubular truss members with a variety of constrained layer damping treatments along its length. The truss member is divided into sections with distinct damping treatments. Each section consists of concentric layers of an outer tube, viscous layer, and inner tube. The equations of motion of a typical section are obtained by Hamilton's principle. An exact solution to the equations is obtained and used to develop the dynamic stiffness matrix for a typical section. A novel condensation and assembly scheme is used to develop a superelement for a truss member comprising multiple sections with the damping treatments. The superelement is verified by comparison of results with an analytical solution and with a conventional finite element model for internal and external constrained layer damping.

I. Introduction

LARGE-SPACE structures are, typically, composed of repetitive truss substructures. They are necessarily built large in size with slender members to save material. Because of their inherent flexibility, these structures are exceptionally susceptible to vibration. In the presence of such vibration, structures in orbit may not satisfy their mission requirements. For example, pointing requirements are needed for successful signal transmission. Therefore, it is of primary importance to minimize the vibration of large-space structures.

Vibration control of large-space structures can be achieved by active and/or passive techniques. Active control requires the use of externally mounted sensors and actuators and appropriate control algorithms. Control–structure interaction and unintentional spillover are important considerations in the design of an active control system. In a passive technique, the damping of a structure is typically augmented by incorporating high-damping material in the structure. For truss structures, augmented damping in the joints and members is possible.

The effect of joint damping has been studied by Crawley,[1] Belvin,[2] and Bowden and Dugundji.[3] Member damping has been investigated by several authors using various analytical methods. Sun and Juang[4] and Abrate and Sun[5] studied the damping of truss structures using a continuum approach. McTavish et al.[6] and McTavish and Hughes[7] utilize a minioscillator mechanical analogy to model member damping in trusses. In both approaches, the damping parameters are calibrated to match inherent and/or augmented damping properties.

Augmented member damping is typically achieved using a constrained layer of high-damping material. Numerous variations of the damping layers' lengths, thicknesses, and configurations are possible. Because of the large number of design possibilities, it is desirable to develop an analytical technique that is capable of predicting the damping achieved for a variety of constrained layer damping treatments. Sun et al.[8] utilized an offset beam element and two-dimensional elements to model a beam with constrained layer damping. Because of the small thickness of the damping layer relative to the beam length, large-element aspect ratios were required to model the damping layer using two-dimensional elements. Because of this difficulty, conventional finite element modeling of constrained layer damping treatments is not an appropriate design tool.

He and Rao[9] developed an exact dynamic stiffness matrix for an adhesively bonded lap joint and studied the effects of damping on the structural behavior. The model studied by He and Rao is limited to only one configuration. Sankar and Deshpande[10] also utilized the dynamic stiffness matrix to evaluate natural frequencies, mode shapes, and modal loss factor of a truss with several viscously damped members. Modeling a bar with segmented damping treatments is achieved. This approach provides an efficient method to evaluate response of bars with a variety of damping treatments. In the study, however, the mass and, hence, the kinetic energy of the viscous layer were neglected.

In the current work, an approach similar to that presented by He and Rao[9] is used to derive the exact dynamic stiffness matrix for concentric circular tubes containing a constrained damping layer. A novel condensation scheme is used to allow for internal or external damping layer configurations. Concentric tube sections are then assembled to obtain the equations of a superelement representing a tubular truss member with segmented damping of arbitrary configuration. The results of the superelement are verified by comparison with an analytical solution for a single-degree-of-freedom (SDOF) oscillator and with a conventional finite element model.

The dynamic stiffness matrix for the superelement can easily be incorporated in a general finite element code to allow for modeling of damped truss members in a large-space structure. Since the computational effort required to form the superelement is negligible, its use does not increase the computational time required for analysis of the large-space structure. Alternately, one can model the damped truss member using conventional finite element analysis; however, each model requires a large number of elements. In a preliminary stage of design, many parameters may vary (such as lengths, thicknesses, and configurations) requiring a large number of models to be generated. Therefore, conventional finite element modeling of damped truss members will, in general, add significant computational effort to the analysis of large-space structures. Although conventional modeling is computationally intensive, it allows for modeling of more complex geometry that may be desirable for the final design.

II. Formulation

A typical damping treated section of the truss member consists of a concentric inner tube, viscoelastic layer, and outer tube as shown in Fig. 1. It is assumed that each layer is linear elastic and isotropic and that damping is included in the viscoelastic layer through the use of a loss factor and complex modulus of elasticity. To utilize Hamilton's principle, expressions for the kinetic energy and strain energy in cylindrical coordinates will be specialized for the kinematic assumptions for the concentric tube system. The kinetic energy T and strain energy U are written as

$$T = \frac{1}{2}\int \rho(\dot{u}^2 + \dot{v}^2 + \dot{w}^2) r \, dr \, d\theta \, dz \tag{1}$$

Received April 21, 1995; revision received July 29, 1995; accepted for publication July 31, 1995.

*Teaching and Research Assistant, Department of Civil and Environmental Engineering; currently Project Manager, BVH Engineers, Inc., Bloomfield, CT 06002.

†Assistant Professor, Department of Civil and Environmental Engineering. Member AIAA.

‡Associate Professor, Department of Civil and Environmental Engineering.

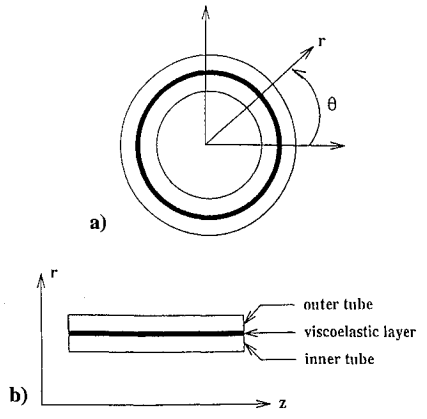

Fig. 1 Typical section of a truss member: a) cross section and b) axisymmetric section.

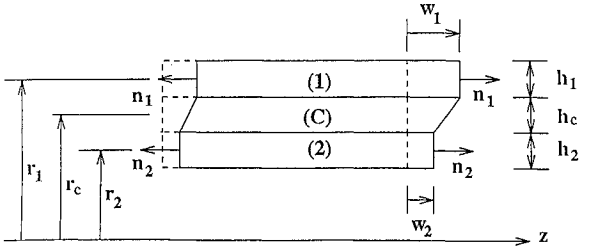

Fig. 2 Kinematic assumptions and free body diagram of a section.

$$U = \frac{1}{2}\int (\sigma^T \epsilon) r \, dr \, d\theta \, dz \tag{2}$$

where u, v, and w are displacements in the radial, circumferential, and axial directions, respectively; σ and ϵ are the vectors of stress and strain components, respectively; and ρ is the density of the material. An overdot on a character indicates the time derivative of the corresponding parameter.

Next, the kinematic assumptions for each layer of the concentric tube section are incorporated in the kinetic and strain energy expressions. Figure 2 shows the kinematic assumptions and geometric parameters of the section. For the outer tube (subscript 1), the kinematic assumptions are

$$u(r, \theta, z) = v(r, \theta, z) = 0 \tag{3a}$$

$$w(r, \theta, z) = w_1(z) \tag{3b}$$

Similarly, for the inner tube (subscript 2)

$$u(r, \theta, z) = v(r, \theta, z) = 0 \tag{4a}$$

$$w(r, \theta, z) = w_2(z) \tag{4b}$$

For the viscoelastic layer (subscript c), the axial displacement is assumed to vary linearly in the radial direction

$$u(r, \theta, z) = v(r, \theta, z) = 0 \tag{5a}$$

$$w(r, \theta, z) = w_c(r, z) = \frac{w_1 + w_2}{2} + \frac{w_1 - w_2}{h_c}(r - r_c) \tag{5b}$$

where r_c and h_c are the radius and the thickness of the viscoelastic layer.

A. Kinetic Energies

The total kinetic energy of the section is the sum of the kinetic energies for each layer. For each layer $u = v = 0$ and $w = w(r, z)$, therefore, Eq. (1) can be simplified to

$$T = \pi \int_z \int_r \rho \dot{w}^2 r \, dr \, dz \tag{6}$$

For the outer layer (radius r_1 and thickness h_1), using the assumptions given in Eq. (3) and integrating from $r = r_1 - h_1/2$ to $r = r_1 + h_1/2$ results in

$$T_1 = \int_z \pi \rho_1 r_1 h_1 \dot{w}_1^2 \, dz \tag{7}$$

Similarly, using Eq. (4) for the inner tube (radius r_2 and thickness h_2) yields

$$T_2 = \int_z \pi \rho_2 r_2 h_2 \dot{w}_2^2 \, dz \tag{8}$$

For the viscoelastic layer (radius r_c and thickness h_c), using the assumptions given in Eq. (5) and integrating from $r = r_c - h_c/2$ to $r = r_c + h_c/2$ results in

$$T_c = \int_z \pi \rho_c \left[a \dot{w}_1^2 + b \dot{w}_2^2 + c \dot{w}_1 \dot{w}_2 \right] dz \tag{9}$$

where

$$a = \frac{4 r_c h_c + h_c^2}{12} \tag{10a}$$

$$b = \frac{4 r_c h_c - h_c^2}{12} \tag{10b}$$

$$c = \frac{4 r_c h_c}{12} \tag{10c}$$

B. Strain Energies

The total strain energy of the section is the sum of the strain energies for each layer. For each layer $u = v = 0$ and $w = w(r, z)$, therefore, Eq. (2) can be simplified to

$$U = \pi \int_z \int_r [\sigma_{zz} \epsilon_{zz} + \sigma_{rz} \gamma_{rz}] r \, dr \, dz \tag{11}$$

where σ_{zz} and ϵ_{zz} are the normal stress and strain, respectively, in the z direction; and σ_{rz} and γ_{rz} are the shearing stress and strain, respectively, in the r–z plane. The constitutive relation is assumed to be isotropic in each layer; therefore

$$\sigma_{zz} = \frac{E(1 - \nu)}{(1 + \nu)(1 - 2\nu)} \epsilon_{zz} \qquad \sigma_{rz} = \frac{E}{2(1 + \nu)} \gamma_{rz} \tag{12}$$

where E and ν are the modulus of elasticity and Poisson's ratio, respectively. Damping is included in the viscoelastic layer using a complex modulus of elasticity

$$E_c = E_c^0 (1 + i\eta) \tag{13}$$

where η is the loss factor and E_c^0 is the storage modulus of elasticity of the viscous material.

For the outer tube $\gamma_{rz} = 0$ and $w = w_1(z)$. Performing the r integration in Eq. (11) yields

$$U_1 = \int_z A_1 r_1 h_1 w_1'^2 \, dz \tag{14}$$

where

$$A_1 = \frac{\pi E_1 (1 - \nu_1)}{(1 + \nu_1)(1 - 2\nu_1)} \tag{15}$$

A prime on a character indicates the derivative of the corresponding quantity with respect to z.

Similarly, for the inner tube, the strain energy becomes

$$U_2 = \int_z A_2 r_2 h_2 w_2'^2 \, dz \tag{16}$$

where A_2 is given by the relation similar to Eq. (15). For the viscoelastic layer, ϵ_{zz} and γ_{rz} are found using the kinematic assumptions given by Eq. (5). The resulting strain energy is written as

$$U_c = \int_z \left[A_c \left(a w_1'^2 + b w_2'^2 + c w_1' w_2' \right) + \frac{\pi G_c r_c}{h_c} (w_1 - w_2)^2 \right] dz \tag{17}$$

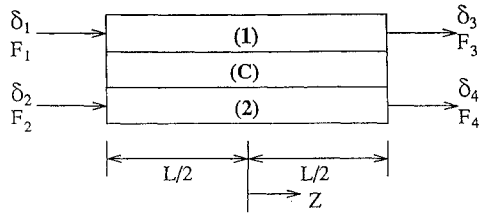

Fig. 3 End forces and displacements on a section.

where A_c is given by the relation similar to Eq. (15) and G_c is the complex shear modulus of the viscous layer.

C. Hamilton's Principle

Hamilton's principle is written as

$$\delta \int_{t_1}^{t_2} (T - U + W_{\text{ext}})\, dt = 0 \tag{18}$$

where W_{ext} is the work of external loads and δ is the variational operator. The work term due to axial loads $n(z, t)$, at each end of the outer and inner tubes as shown in Fig. 2, is

$$W = -n_1 w_1|_{z=-L/2} + n_1 w_1|_{z=+L/2} - n_2 w_2|_{z=-L/2} + n_2 w_2|_{z=+L/2} \tag{19}$$

Combining the expressions for the kinetic energies, strain energies, and work for the outer tube, viscoelastic layer, and inner tube gives the following expression of Hamilton's principle:

$$\delta \int_{t_1}^{t_2} \left[\int_z \left[\left\{ \pi\rho_1 r_1 h_1 \dot{w}_1^2 + \pi\rho_2 r_2 h_2 \dot{w}_2^2 + \pi\rho_c \left(a\dot{w}_1^2 + b\dot{w}_2^2 + c\dot{w}_1\dot{w}_2 \right) \right\} - \left\{ A_1 r_1 h_1 w_1'^2 + A_2 r_2 h_2 w_2'^2 + \left[A_c \left(a w_1'^2 + b w_2'^2 + cA w_1' w_2' \right) + (\pi G_c r_c / h_c)(w_1 - w_2)^2 \right] \right\} \right] dz - (n_1 w_1 + n_2 w_2)|_{z=-L/2} + (n_1 w_1 + n_2 w_2)|_{z=+L/2} \Bigg] dt = 0 \tag{20}$$

Performing the variation on $w_1(z, t)$ and $w_2(z, t)$ and integrating by parts[11] yields the following equations of motion and natural boundary conditions for the concentric tube system:

$$2(A_1 r_1 h_1 + A_c a) w_1'' + A_c c w_2'' - 2\pi(\rho_1 r_1 h_1 + \rho_c a)\ddot{w}_1 - \pi\rho_c c \ddot{w}_2 - (2\pi G_c r_c / h_c)(w_1 - w_2) = 0 \tag{21}$$

$$2(A_2 r_2 h_2 + A_c b) w_2'' + A_c c w_1'' - 2\pi(\rho_2 r_2 h_2 + \rho_c b)\ddot{w}_2 - \pi\rho_c c \ddot{w}_1 - (2\pi G_c r_c / h_c)(w_2 - w_1) = 0 \tag{22}$$

$$[2(A_1 r_1 h_1 + A_c a) w_1' + c A_c w_2' - n_1]\delta w_1|_{z=\pm L/2} = 0 \tag{23}$$

$$[2(A_2 r_2 h_2 + A_c b) w_2' + c A_c w_1' - n_2]\delta w_2|_{z=\pm L/2} = 0 \tag{24}$$

D. Harmonic Solution

The harmonic time-dependent solution is obtained by assuming w_1, w_2, n_1, and n_2 in the following form:

$$w_1(z, t) = W_1(z) e^{i\omega t} \tag{25a}$$

$$w_2(z, t) = W_2(z) e^{i\omega t} \tag{25b}$$

$$n_1(z, t) = N_1(z) e^{i\omega t} \tag{25c}$$

$$n_2(z, t) = N_2(z) e^{i\omega t} \tag{25d}$$

Substituting these expressions into the equations of motion yields

$$(J_1 D^2 + K_1) W_1 + (L D^2 + M) W_2 = 0 \tag{26}$$

$$(L D^2 + M) W_1 + (J_2 D^2 + K_2) W_2 = 0 \tag{27}$$

where

$$D^2() = \frac{d^2()}{dz^2} \tag{28}$$

and

$$J_1 = 2(A_1 r_1 h_1 + A_c a) \tag{29a}$$

$$J_2 = 2(A_2 r_2 h_2 + A_c b) \tag{29b}$$

$$L = c A_c \tag{30a}$$

$$M = \pi \left[\omega^2 c \rho_c + \frac{2 G_c r_c}{h_c} \right] \tag{30b}$$

$$K_1 = 2\pi \left[\omega^2 (\rho_1 r_1 h_1 + \rho_c a) - (G_c r_c / h_c) \right] \tag{31a}$$

$$K_2 = 2\pi \left[\omega^2 (\rho_2 r_2 h_2 + \rho_c b) - (G_c r_c / h_c) \right] \tag{31b}$$

Assuming a solution of the form

$$W_1(z) = A_1^* \cosh(\lambda_1 z) + A_2^* \sinh(\lambda_1 z) + A_3^* \cosh(\lambda_2 z) + A_4^* \sinh(\lambda_2 z) \tag{32}$$

$$W_2(z) = A_1^* f_1 \cosh(\lambda_1 z) + A_2^* f_1 \sinh(\lambda_1 z) + A_3^* f_2 \cosh(\lambda_2 z) + A_4^* f_2 \sinh(\lambda_2 z) \tag{33}$$

Equations (26) and (27) give

$$\lambda_1^2, \lambda_2^2 = \frac{-(J_1 K_2 + J_2 K_1 - 2LM) \pm \sqrt{(J_1 K_2 + J_2 K_1 - 2LM)^2 - 4(J_1 J_2 - L^2)(K_1 K_2 - M^2)}}{2(J_1 J_2 - L^2)} \tag{34}$$

$$f_i = \frac{-(J_1 \lambda_i^2 + K_1)}{(L\lambda_i^2 + M)} \qquad i = 1, 2 \tag{35}$$

E. Dynamic Stiffness Matrix

The dynamic stiffness matrix for the concentric tube section is found using the exact harmonic solution by prescribing the end displacements (δ_i, $i = 1, 4$) and end forces (F_i, $i = 1, 4$), as shown in Fig. 3. First, the following displacement boundary conditions are prescribed:

$$W_1(-L/2) = \delta_1 \tag{36a}$$

$$W_2(-L/2) = \delta_2 \tag{36b}$$

$$W_1(L/2) = \delta_3 \tag{36c}$$

$$W_2(L/2) = \delta_4 \tag{36d}$$

Substituting for W_1 and W_2 from Eqs. (32) and (33) gives

$$\begin{Bmatrix} \delta_1 \\ \delta_2 \\ \delta_3 \\ \delta_4 \end{Bmatrix} = \begin{bmatrix} C_1 & -S_1 & C_2 & -S_2 \\ f_1 C_1 & -f_1 S_1 & f_2 C_2 & -f_2 S_2 \\ C_1 & S_1 & C_2 & S_2 \\ f_1 C_1 & f_1 S_1 & f_2 C_2 & f_2 S_2 \end{bmatrix} \begin{Bmatrix} A_1^* \\ A_2^* \\ A_3^* \\ A_4^* \end{Bmatrix} \tag{37}$$

where

$$C_i = \cosh(\lambda_i L/2) \tag{38a}$$

$$S_i = \sinh(\lambda_i L/2) \qquad i = 1, 2 \tag{38b}$$

Equation (37) can be inverted to yield

$$\begin{Bmatrix} A_1^* \\ A_2^* \\ A_3^* \\ A_4^* \end{Bmatrix} = \frac{1}{2(f_1 - f_2)} \begin{bmatrix} -\frac{f_2}{C_1} & \frac{1}{C_1} & -\frac{f_2}{C_1} & \frac{1}{C_1} \\ \frac{f_2}{S_1} & -\frac{1}{S_1} & -\frac{f_2}{S_1} & \frac{1}{S_1} \\ \frac{f_1}{C_2} & -\frac{1}{C_2} & \frac{f_1}{C_2} & -\frac{1}{C_2} \\ -\frac{f_1}{S_2} & \frac{1}{S_2} & \frac{f_1}{S_2} & -\frac{1}{S_2} \end{bmatrix} \begin{Bmatrix} \delta_1 \\ \delta_2 \\ \delta_3 \\ \delta_4 \end{Bmatrix} \tag{39}$$

which is written simply as $\boldsymbol{A}^* = \boldsymbol{R}\boldsymbol{\delta}$.

The axial forces in the outer and inner tubes are found from Eqs. (23), (24), and (29)

$$N_1(z) = J_1 W_1' + L W_2' \tag{40a}$$

$$N_2(z) = L W_1' + J_2 W_2' \tag{40b}$$

The following force boundary conditions are prescribed:

$$N_1(-L/2) = -F_1 \tag{41a}$$

$$N_2(-L/2) = -F_2 \tag{41b}$$

$$N_1(L/2) = F_3 \tag{41c}$$

$$N_2(L/2) = F_4 \tag{41d}$$

The resulting boundary conditions can be written as

$$\begin{Bmatrix} F_1 \\ F_2 \\ F_3 \\ F_4 \end{Bmatrix} = \begin{bmatrix} d_1 S_1 & -d_1 C_1 & d_2 S_2 & -d_2 C_2 \\ d_3 S_1 & -d_3 C_1 & d_4 S_2 & -d_4 C_2 \\ d_1 S_1 & d_1 C_1 & d_2 S_2 & d_2 C_2 \\ d_3 S_1 & d_3 C_1 & d_4 S_2 & d_4 C_2 \end{bmatrix} \begin{Bmatrix} A_1^* \\ A_2^* \\ A_3^* \\ A_4^* \end{Bmatrix} \tag{42}$$

where

$$d_1 = \lambda_1(J_1 + L f_1) \tag{43a}$$

$$d_2 = \lambda_2(J_1 + L f_2) \tag{43b}$$

$$d_3 = \lambda_1(J_2 f_1 + L) \tag{43c}$$

$$d_4 = \lambda_2(J_2 f_2 + L) \tag{43d}$$

Equation (42) is written simply as $\boldsymbol{F} = \boldsymbol{S}\boldsymbol{A}^*$. The dynamic stiffness matrix $\boldsymbol{D}$ is obtained by combining Eqs. (42) and (39) as follows:

$$\boldsymbol{F} = \boldsymbol{D}\boldsymbol{\delta} \tag{44a}$$

$$\boldsymbol{D} = \boldsymbol{S}\boldsymbol{R} \tag{44b}$$

Equation (44) contains 4 DOF. The concentric tube section is typically connected at two ends and is free at the remaining two ends. The last step in the derivation is to order the DOF, partition the 4×4 dynamic stiffness matrix, and condense out the DOF associated with the free ends. The ordering puts the DOF at connected ends in rows 1 and 2, and DOF at free ends in rows 3 and 4. For example, if the outer tube is connected at the left and free on the right ($F_3 = 0$), and the inner tube is connected at the right and free at the left ($F_2 = 0$) then Eq. (44) is ordered and partitioned as

$$\begin{Bmatrix} F_1 \\ F_4 \\ 0 \\ 0 \end{Bmatrix} = \begin{bmatrix} \boldsymbol{D}_{11} & \boldsymbol{D}_{12} \\ \boldsymbol{D}_{21} & \boldsymbol{D}_{22} \end{bmatrix} \begin{Bmatrix} \delta_1 \\ \delta_4 \\ \delta_2 \\ \delta_3 \end{Bmatrix} \tag{45}$$

This ordering is written as (1, 3, 4, 2).

Condensing out δ_2 and δ_3 yields the following 2×2 dynamic stiffness matrix for the section

$$\begin{Bmatrix} F_1 \\ F_4 \end{Bmatrix} = \begin{bmatrix} \boldsymbol{D}_{11} & -\boldsymbol{D}_{12} & \boldsymbol{D}_{22}^{-1} & \boldsymbol{D}_{21} \end{bmatrix} \begin{Bmatrix} \delta_1 \\ \delta_4 \end{Bmatrix} \tag{46}$$

The ordering is specified for each section, which allows them to be connected in different configurations along the truss member length. This feature provides tremendous versatility in modeling truss members with a variety of damping treatments. The dynamic stiffness matrices for each section are then assembled to find the equations for the superelement representing the damped truss member.

III. Verification

The solution presented in Sec. II is verified by comparison with an analytical solution for a SDOF oscillator and with a conventional finite element model.

A. Comparison with SDOF Oscillator

Three sections are assembled as shown in Fig. 4. The first section consists of a rigid massless outer tube. The second section consists of a rigid massless outer tube, a viscoelastic massless layer, and a rigid inner tube with mass. The third section consists of a rigid inner tube with mass. This structure is fixed at the left end and loaded by a harmonic force at the right end. Because of the assumed properties, the structure will behave as a SDOF oscillator. The geometric and material properties used are given in Tables 1 and 2, respectively. The section lengths are $L_1 = 7.62$ cm (3 in.), $L_2 = 15.24$ cm (6 in.), and $L_3 = 7.62$ cm (3 in.).

The mass of the SDOF oscillator is

$$M = 2\pi r_2 h_2 (L_2 + L_3)\rho_2 \tag{47}$$

The shearing stress τ acting at the interface between the viscoelastic layer and inner tube is

$$\tau = G_c \gamma = G_c(\delta/h_c) \tag{48}$$

where G_c is the shear modulus of the viscous material and δ is the axial deformation. For a constant shear stress, the total force F is

$$F = 2\pi\left(\frac{r_c + r_2}{2}\right) L_2 \tau = \frac{\pi(r_c + r_2) L_2 G_c}{h_c}\delta = k\delta \tag{49}$$

where k is the spring constant of the SDOF oscillator. Since the shear modulus of the viscoelastic layer includes loss factor damping, the spring constant k is complex:

$$k = k_R + i k_I = \frac{\pi(r_c + r_2) L_2 G_c^0}{h_c}(1 + i\eta) \tag{50}$$

where G_c^0 is the storage shear modulus of the viscoelastic material.

Table 1 Geometric properties for the three-section structure

	Thickness, cm			Radius, cm		
Section	h_1	h_c	h_2	r_1	r_c	r_2
1, 2, 3	0.254	0.254	0.254	15.24	15.00	14.73

Table 2 Material properties for the SDOF oscillator

	Young's modulus, GPa			Mass density, kg/m^3			Poisson's ratio		
Section	E_1	E_c	E_2	ρ_1	ρ_c	ρ_2	ν_1	ν_c	ν_2
1	69	0	0	0	0	0	0.3	0	0
2	69	69×10^{-5}	69	0	0	2800	0.3	0.3	0.3
3	0	0	69	0	0	2800	0	0	0.3

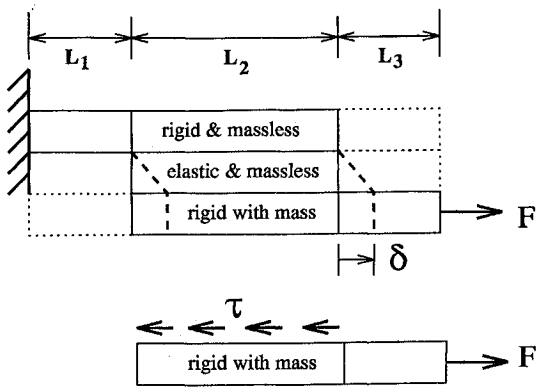

Fig. 4 Three-segment structure reduced to a SDOF oscillator.

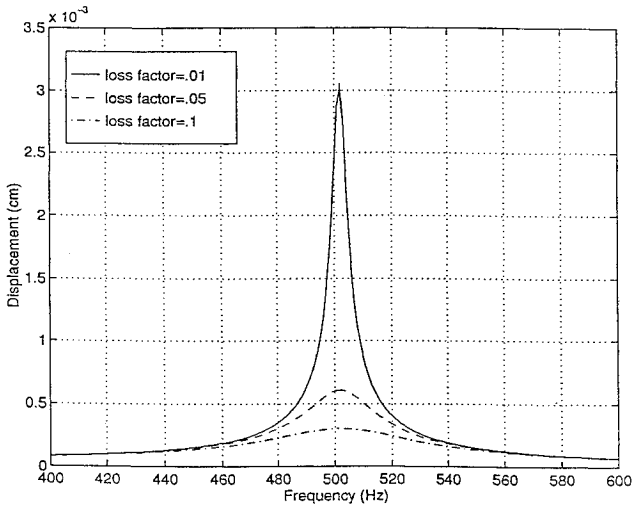

Fig. 5 Verification with a SDOF oscillator: displacement vs frequency.

The natural frequency ω_n of the SDOF oscillator is

$$\omega_n = \sqrt{k_R/M} \tag{51}$$

The displacement of the SDOF oscillator is found from

$$\left(k_R + ik_I - \omega^2 M\right)\delta = F \tag{52}$$

When $\omega = \omega_n$, the magnitude of the displacement is

$$|\delta| = \frac{F}{k_I} = \frac{Fh_c}{\pi(r_2 + r_c)L_2 G_c^0 \eta} \tag{53}$$

Substituting values from Table 1 into Eqs. (51) and (53) and using $F = 4.448$ N (1.0 lb) gives

$$\omega_n = 502 \text{ Hz} \tag{54a}$$

$$|\delta| = \frac{1}{33395\eta} \text{ cm} \tag{54b}$$

In Fig. 5, the displacement vs frequency of the three-section structure is shown for three values of the loss factor. The natural frequency predicted by the present solution agrees closely with that of the SDOF oscillator. As the damping is increased, the magnitude of the displacement at the natural frequency decreases. In Fig. 6, the magnitude of the displacement at the natural frequency vs loss factor is plotted for the present solution and for the SDOF oscillator. Excellent agreement is obtained.

B. Comparison with Conventional Finite Element Model

In the preceding section, the new solution was verified by reducing a three-section structure to a SDOF oscillator. For this case, the stresses and displacements are constant along each section's length. To further verify the present solution and identify its limitations, a comparison with a conventional finite element model was performed. The three-section structures shown in Fig. 7 were analyzed. In Fig. 7a, the damping layer is internal, whereas in Fig. 7b the damping layer is external. Two different section lengths were considered. In the first case, $L_1 = L_2 = L_3 = 152.4$ cm (60 in.), which gives damping over 33% of the total length, and in the second case, $L_1 = 114.3$ (45 in.), $L_2 = 228.6$ cm (90 in.), and $L_3 = 114.3$ cm (45 in.), which corresponds to 50% damping. The geometric and material properties given in Tables 1 and 3, respectively, were used for all cases. The loss factor (η) is considered to be 0.1.

Table 3 Material properties for verification cases 1 and 2

Section	Young's modulus, GPa			Mass density, kg/m^3			Poisson's ratio		
	E_1	E_c	E_2	ρ_1	ρ_c	ρ_2	ν_1	ν_c	ν_2
1	69	0	0	2800	0	0	0.3	0	0
2	69	2.07	69	2800	2800	2800	0.3	0.3	0.3
3	0	0	69	0	0	2800	0	0	0.3

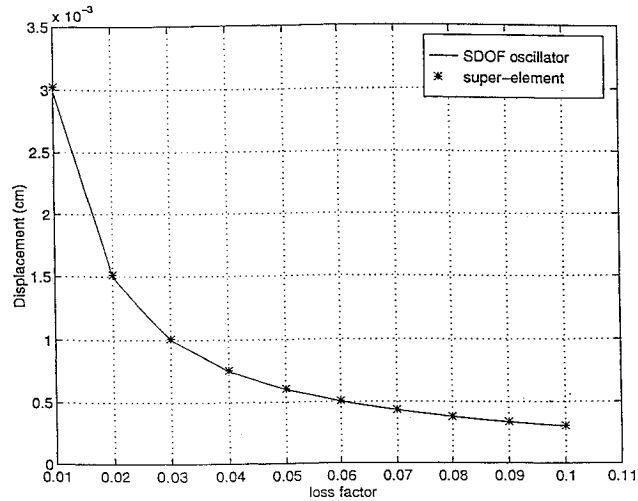

Fig. 6 Verification with a SDOF oscillator: displacement vs loss factor.

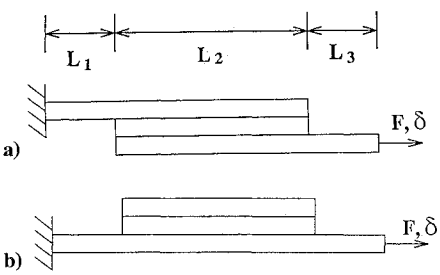

Fig. 7 Three-segment structure: a) internal damping and b) external damping.

The finite element analysis was performed using MARC. Two-dimensional axisymmetric solid elements were used. One element was used through the thickness of each layer. Element aspect ratios were kept at $\Delta z{:}\Delta r = 1{:}1$ near the ends of each section and increased to $\Delta z{:}\Delta r = 5{:}1$ in the interior of each section. The models required approximately 1000 elements for cases 1 and 2.

Because of the eccentricity of the loading and interface shear, bending is introduced in the structure. Bending effects were neglected in the kinematic assumptions for the present solution. To study the effects of bending on the response, two different finite element analyses were performed. In the first, only the nodes at the left and right ends of the model were constrained radially and all interior nodes were radially unconstrained (RU). In the second, all nodes were radially constrained (RC).

Figure 8 shows displacement vs frequency obtained from the current solution for cases 1 (33%) and 2 (50%) with internal damping.

Table 4 Comparison of natural frequencies for case 1 (33%) with internal damping

Mode	Current solution, Hz	MARC RU, Hz	Difference, %	MARC RC, Hz	Difference, %
1	265	228	16.2	265	0.0
2	895	773	15.8	897	0.2
3	1480	1273	16.3	1496	1.1
4	2030	1736	16.9	2018	0.6

Table 5 Comparison of natural frequencies for case 2 (50%) with internal damping

Mode	Current solution, Hz	MARC RU, Hz	Difference, %	MARC RC, Hz	Difference, %
1	255	219	16.4	254	0.4
2	885	763	16.0	886	0.1
3	1395	1210	15.3	1407	0.9
4	2005	1725	16.2	2015	0.5

Table 6 Comparison of natural frequencies for case 1 (33%) with external damping

Mode	Current solution, Hz	MARC RU, Hz	Difference, %	MARC RC, Hz	Difference, %
1	260	225	15.6	261	0.4
2	895	773	15.8	897	0.2
3	1485	1276	16.4	1501	1.1
4	2025	1735	16.7	2013	0.6

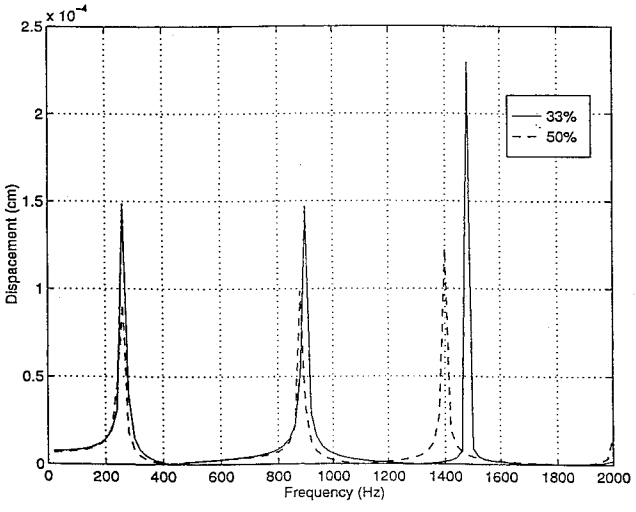

Fig. 8 Displacement vs frequency for cases 1 and 2 with internal damping.

Small shifts in the natural frequencies occur due to the difference in stiffness and mass of the two cases. For the two cases considered, different levels of damping occur for the first three modes. Tables 4 and 5 summarize the natural frequencies predicted by the current solution and the RU and RC MARC models for cases 1 and 2, respectively. For the RU model, the difference in natural frequencies is approximately 17% for the two cases considered. For the RC model, the results agree within 1%.

Figure 9 shows displacement vs frequency for cases 1 (33%) and 2 (50%) with external damping. Tables 6 and 7 summarize the predicted natural frequencies. The predicted natural frequencies agree within 17% for the RU model and within 1% for the RC model.

It is expected that the importance of bending will depend on the geometric and material parameters of the structure, which can be further investigated by additional parametric studies. Bending can be included in the kinematic assumptions and the same solution procedure can be applied; however, the complexity of the equations will increase significantly.

Table 7 Comparison of natural frequencies for case 2 (50%) with external damping

Mode	Current solution, Hz	MARC RU, Hz	Difference, %	MARC RC, Hz	Difference, %
1	250	217	15.2	251	0.4
2	885	762	16.1	885	0.0
3	1395	1211	15.2	1408	0.9
4	2010	1730	16.2	2020	0.5

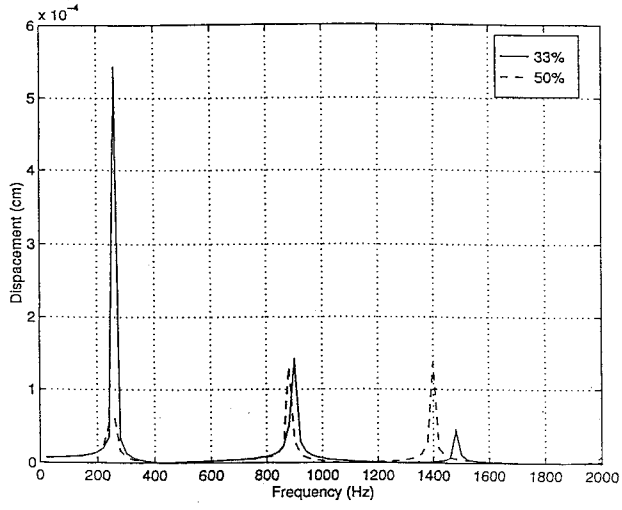

Fig. 9 Displacement vs frequency for cases 1 and 2 with external damping.

IV. Conclusions

The exact dynamic stiffness matrix is determined for a tubular section consisting of a concentric outer tube, viscoelastic layer, and inner tube. The dynamic stiffness matrix can be assembled to form a truss member with multiple sections with different damping configurations. The solution was verified by comparison of results with the analytical solution for a SDOF oscillator and with a conventional finite element model. Comparison with the finite element model showed that bending occurs in the sections, which is not included in the kinematic assumptions of the present solution. The solution can be modified to include bending, but the complexity of the equations will increase significantly.

The solution developed provides an efficient technique to model large-space structures comprising tubular truss members with a variety of constrained layer damping treatments. The dynamic response of large-space structures with damping will be examined in a forthcoming publication by the authors.

Acknowledgment

This work was partly funded by the NASA/Connecticut Space Grant College Consortium. The support is gratefully acknowledged.

References

[1]Crawley, E. F., "Nonlinear Characteristics of Joints as Elements of Multi-Body Dynamic Systems," *Computational Methods for Structural Mechanics and Dynamics*, NASA CP 3034, 1989, pp. 543–588.

[2]Belvin, W. K., "Modeling of Joints for the Dynamic Analysis of Truss Structures," NASA TP 2661, May 1987.

[3]Bowden, M., and Dugundji, J., "Effects of Joint Damping and Joint Nonlinearity on the Dynamics of Space Structures," AIAA Paper 88-2480, April 1988.

[4]Sun, C. T., and Juang, J. N., "Modeling Global Structural Damping in Trusses Using Simple Continuum Models," AIAA Paper 83-1008, May 1983.

[5]Abrate, S., and Sun, C. T., "Continuum Modeling of Damping in Large Space Structures," *Proceedings of the Second International Conference on*

the Recent Advances in Structural Dynamics, Vol. 2, edited by M. Petyt and H. F. Wolfe, Univ. of Southampton, Southampton, England, UK, 1984, pp. 877–885.

[6]McTavish, D. J., Hughes, P. C., Soucy, Y., and Graham, W. B., "Prediction and Measurement of Modal Damping Factors for Viscoelastic Space Structures," *AIAA Journal*, Vol. 30, No. 5, 1992, pp. 1392–1399.

[7]McTavish, D. J., and Hughes, P. C., "Modeling of Linear Viscoelastic Space Structures," *Journal of Vibration and Acoustics*, Vol. 115, Jan. 1993, pp. 103–110.

[8]Sun, T. C., Sankar, B. V., and Rao, V. S., "Damping and Vibration Control of Unidirectional Composite Laminates Using Add-on Viscoelastic Materials," *Journal of Sound and Vibration*, Vol. 139, No. 2, 1990, pp. 227–287.

[9]He, S., and Rao, M. D., "Longitudinal Vibration and Damping Analysis of Adhesively Bonded Double-Strap Joints," *Journal of Vibration and Acoustics*, Vol. 114, July 1992, pp. 330–337.

[10]Sankar, B., and Deshpande, A. S., "Passive Damping of Large Space Structures," *AIAA Journal*, Vol. 31, No. 8, 1993, pp. 1511–1516.

[11]Adib-Jahromi, H., "Passive Damping of Truss Structures with Tubular Members," Ph.D. Dissertation, Dept. of Civil and Environmental Engineering, Univ. of Connecticut, Storrs, CT, March 1995.